

Evaluation of Pavement Stripping Using Ground Penetrating Radar – A Case Study

Kasinathan Muthukkumar¹[0000-0002-7664-7068], Nandhagopal Raja²[0000-0002-5311-9836],
and Umanath Umaian³[0000-0003-4798-971X]

¹Professor, Department of Civil Engineering, National Institute of Technology,
Tiruchirappalli - 620015

^{2,3}Research Scholar, Department of Civil Engineering, National Institute of Technology,
Tiruchirappalli - 620015
kmk@nitt.edu

Abstract. Non-destructive testing techniques are highly valuable in the present day scenario as it can save money and time for the qualitative evaluation of any site. This paper presents a case study utilizing one such technique, employing a ground-coupled Ground Penetrating Radar (GPR). The GPR was used to estimate the damages to the pavement and underlying subgrade soil at Cochin International Airport Limited (CIAL), Cochin, Kerala, India. The state of Kerala received 75% more than expected rainfall in the monsoon of 2018 and hence, faced one of the worst natural disasters in the form of floods between July and August. Therefore, a subsurface survey was performed at CIAL to analyse the pavement area and identify any detrimental effects caused by the floods. The subsurface survey scope was to image the subsurface to an approximate depth of 2-3m to map the anomalies and quantitatively evaluate the affected areas of the runway, taxiways, and the link-ways. Non-destructive testing was opted not to affect the regular operations at the airport. This investigation involved the use of remote measurement methods, and therefore, all the findings presented here are the result of the measurement and interpretation of GPR data. The analysis was performed using a dedicated data analytics software called RADAN7. Based on the analysis, a quantitative criterion called the “stripping index” has been computed to define the degree of damages sustained by the pavement and its underlying layers. The results are both graphically and quantitatively discussed in this paper.

Keywords: Ground Penetrating Radar; Runway pavement; Non-destructive testing; Stripping index; Pavement debonding.

1 Introduction

Ground Penetrating Radar (GPR) is a subsurface imaging device. GPR uses electromagnetic radiation of frequencies falling in the radio spectrum to transmit, receive, and eventually develop the subsurface image. In general, the radar pulses travel through the sub-surface material at a velocity proportional to that media’s electrical characteristics. The propagation (and reflection) of the radar impulse depends on the di-electrical properties of the groundmass being investigated, and therefore, the presence of any moisture content dramatically influences it.

It works by sending a tiny pulse of energy into the subsurface from the ground level and records the reflected signals' strength and the time taken for its return. A series of such cycles over an area make up a scan. Reflections are produced whenever the energy pulse enters into a material with different electrical conduction properties or dielectric permittivity from the material it passes through. The strength, or amplitude, of the reflection is determined by the contrast of dielectric constants and the two materials' conductivities. This means that a pulse that moves from lower dielectric permittivity to higher dielectric permittivity will produce a very strong reflection. The reverse movement will produce a relatively weak reflection. The saturation due to fluids will dramatically rise in the dielectric of the material, and metals entirely reflect the energy pulses, and the signal cannot pass through.

GPR has several advantages over other NDT methods, and its applications are widespread in the civil engineering domain [1]. The areas of application for ground-penetrating radar are diverse. Notably, its relatively continuous nature of the radar sounding technique makes it an excellent tool to complement shallow exploration [2]. The GPR method can be used to map geologic conditions such as depth of bedrock, depth to the water table [3], soil stratification details such as the depth and thickness of each layer on land, and under freshwater bodies [4]. GPR can also be applied to identify the location of subsurface cavities and fractures in bedrock [5, 6]. Researchers have also established the accuracy of pavement layer thickness measurement by GPR. The thickness values of each layer measured in the GPR radargram were found to be in good agreement with the thickness values measured in a core sample [7, 8, and 9].

Generally, in any flexible pavement, the granular sub-base (GSB) layer is equipped with drains and pipelines to collect and guide the water percolating through the pavement's surface away from the pavement area. This layer is to protect the subgrade soil from any distress due to water percolation. In this case study, the site was subjected to an extreme case of flooding. Although the pavement's surface was not damaged significantly, it was imminent to identify if any damages had been caused to the subgrade soil beneath the pavement. In this case study, three possible applications of GPR are being utilized. Firstly, to identify any debonding on the surface level of the flexible pavement. Secondly, to identify the presence of cavities or water-clogging in the subgrade soil due to the floods. Further, the utilities present beneath the pavement were also located.

The antenna is the critical component of GPR, which influences the performance of the system directly [10]. Most of the research and development work in highway applications have been performed with low frequency 100–500 MHz ground-coupled antennae to evaluate subgrade soils and their interlayers and probe the overburden depth, and survey road structural layers [11]. Therefore, GPR with 400MHz frequency antennae was employed for this study. The equipment was set up on a three-wheeled cart, which was required to be pushed manually. The data was recorded with respect to displacement, measured simultaneously by the equipment being linked with the pedometer equipped on the cart. The data were processed and analysed. The locations of possible de-bonding were manually identified generated GPR radargram. A quantity called "stripping index" was then introduced and estimated based on the wave amplitude data to define the degree of de-bonding numerically [12]. The results generated were both tabulated and graphically developed. The paper discusses the

methodology adopted for this study, the analyses of the collected data, and the interpretations derived.

2 Description of Site - CIAL, Cochin, Kerala, India

Kerala is a place that receives more than the average percentage of rainfall every year. Cochin is majorly affected by the southwest monsoon, which hits in the final week of May or the first week of June. The Northwest monsoons are relatively mild at Cochin, hitting the area in December and extending until March. Therefore, it is a place that receives rainfall round the year but for parts of April and May. In the year 2018, Kerala was subject to torrential rainfall during the southwest monsoon. It was estimated that it received 2346.6mm rainfall against the norm of 1649.5mm, which was approximately 42% more from June to August. Thus, most parts of the state were flooded, and CIAL was also subject to this natural calamity. The floodwater submerged most parts of the runways, taxiways, and link-ways, and the situation sustained for more than a week. Attributing to this reason, all air traffic was suspended. Therefore, it was imminent to verify the quality of the pavement after being subjected to such adverse conditions.

3 GPR Survey

A team of expert personnel visited the site to perform a subsurface investigation of the affected region using the ground-penetrating radar. Firstly, an initial site visit was done to identify areas with visible damages, followed by a systematic GPR survey. The GSSI manufactured ground-coupled GPR device of frequency 400MHz with SIR3000 console was used. This antenna can map the subsurface with maximum accuracy to a depth of 3m under ideal conditions.

We know that the radar waves penetrate through the sub-surface material at velocities proportional to that media's electrical characteristics. In this case, the dielectric constants of the pavement surface and its underlying layers and the subgrade soil differ in values. But, the values of these values lie within a similar range. The range of dielectric constant for the pavement materials, including the asphalt, aggregates, and subgrade soil, lies between 3 to 6. This range is estimated based on the known dielectric constants of common materials [13]. Therefore, an average value of 5 was adopted for the GPR survey for this case study.

4 Data Collection

All the pavement areas that were part of the survey were flexible pavements surfaced with hot mix asphalt overlying the base and subgrade layers. The runway was a total length of 3300m along with east-west orientation and width of 40m, excluding the shoulders. The most visible damage was observed in the central region along the runway's length in the initial site visit. For the ease of conducting the survey, the runway was divided into short segments of length 250m. Further, the GPR was run on the center line and offsets of 5, 10, and 20 meters on either side. The survey was planned in the form of a grid to understand the damages and its flow accurately. The survey was started with the segment at the east end, and it proceeded towards the west. The direction of each run and the corresponding number of the data

Kasinathan Muthukkumaran, Nandhagopal Raj, and Umanath Umaiyan

file was noted down. Figure 1 shows the NITT personnel conducting a GPR survey run on the runway.



Fig.1. GPR Run in the Runway Lane

The parallel taxiway was of a total length of 3400m and a width of 20m, excluding shoulders. Five link-ways connect the parallel taxiway and the runway named C1 to C5 and seven link-ways connecting the apron to the runway, namely, Alpha, Beta, Delta, Echo, Foxtrot, and Golf, and Hotel. All the link-ways were of varying lengths; therefore, they were divided, and the survey was performed as required. Throughout the survey on link-ways, the offsets to the centre line were maintained at 5 and 10 meters on either side. For easy identification of files during the analysis, each survey's direction and the data file names were noted.

5 Data Analysis

Firstly, a general layout diagram was developed, combining the various individual segments of the runway. This diagram also displayed the GPR runs as representative lines at the corresponding chainage, and the file names were labelled. Similar diagrams were developed for the parallel taxiway and each link-way where data collection was performed. For better understanding, a general layout diagram developed for a section of the runway is shown in figure 2. Then, the data collected by the GPR device was transferred to a computer system via hard-drive, and the analysis of the data was performed on the dedicated software RADAN7.

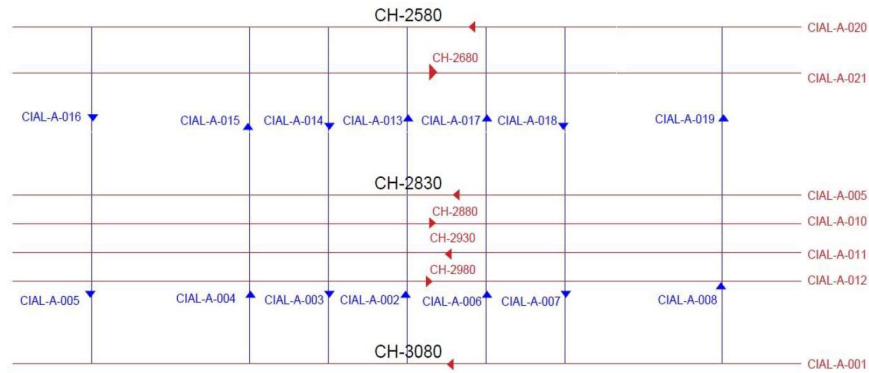


Fig.2. Layout diagram of runs within a segment of the runway

6 Utility Mapping

A data file of a particular run was first imported on to the software interface. Firstly, time zero correction was applied to eliminate the air gap in the interface between the bottom of the GPR device and the ground surface. Secondly, background removal was applied to remove the background noise present as horizontal banding in the data. A frequency-filter was later allowed to run over the data, which eliminated the high-frequency vertical noise. The presence of a hyperbola on the data typically implies the presence of a utility [14]. An example of data showing the presence of a utility in the runway is shown in figure 3. Therefore, the hyperbolas present were identified by visual inspection to which the migration tool was applied to identify the exact depth of the utility. The identified utility was noted down with respect to its chainage and depth functioning as its co-ordinates.

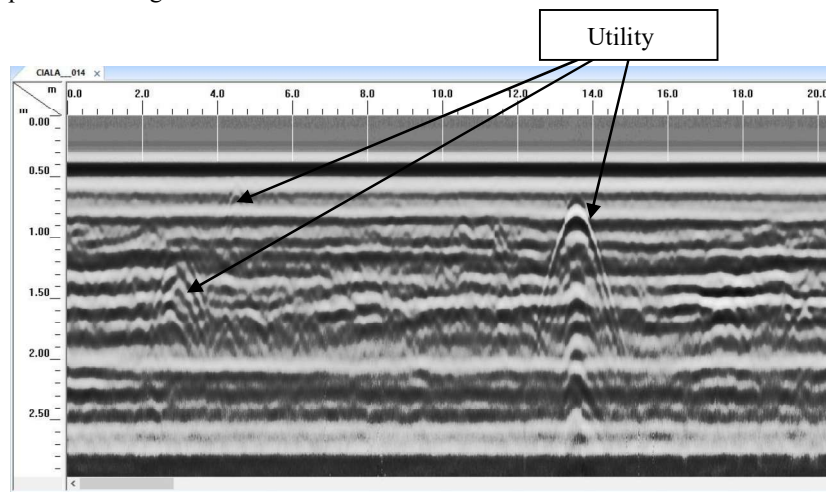


Fig.3. Utility Mapping in the Processed Data File

The locations of the utilities were known data prior to the GPR survey. Therefore, along with the physical measurements of chainage and depth as recorded by the GPR, the existing utilities act as a secondary reference point to estimate the locations of debonding in the recorded radargram with better accuracy.

7 Stripping Index

Debonding in general terms can be expressed as the loss of bonding between the adhesive material and the aggregates due to prolonged interaction of moisture. In the case of the hot mix asphalt, the aggregates and the asphalt lose their bonding. In this study, the water has percolated into the subgrade soil. Therefore, the cavities created due to the waterlogging have also been considered locations of de-bonding in this case study.

Debonding mechanisms have a considerable influence on the residual life of the pavement, and thus their early detection is a very important issue for pavement maintenance [15]. Therefore, this case study is primarily focused on identifying the locations of possible de-bonding on the pavements due to the prolonged presence of moisture. It is also essential to measure the degree of de-bonding at each identified location for immediate solutions to be identified for the same.

A value termed as “Stripping index” quantifies the radar reflection amplitude at each location within a given layer and then measures the uniformity of that value throughout the area analysed [16]. The estimation of the stripping index value is based on the ratio of the average reflection amplitudes obtained through the GPR data processing. As de-bonding occurs non-uniformly in the pavement, the calculation of the stripping index is beneficial in identifying the segments that are likely to be affected. Further, identifying highly affected runs within the segments and identifying and estimating the extent of de-bonding in particular blocks within each run.

8 Calculation of Stripping Index

Generally, a transmitted pulse from the GPR passing from lower dielectric permittivity to higher dielectric permittivity produces a very strong reflection. The opposite movement produces a relatively weak reflection. Saturation due to fluids will cause a dramatic rise in the dielectric of the material in its neighbourhood, creating a stronger reflection. Such strong reflections can be inferred from the processed data by observing for the deeper contrast in colour. The waterlogged cavities in subgrade or debonding of material within the pavement shall also produce a similar effect on the data. Therefore, firstly, the processed data further was visually inspected to identify areas of high contrast, and the chainage and depth of occurrence of such regions were noted. Also, alongside identifying locations of possible de-bonding, the data was studied for any intermixing of the layers beneath the pavement, which could be detrimental to the quality of the pavement. Figure 4 shows a typical example of such a region of suspected debonding alongside areas that remain unaffected. Although the radargram shows the areas of de-bonding, it does not represent the degree of the damages.

Therefore, the value ‘Stripping Index’ has been introduced to represent the degree of debonding quantitatively. For its estimation, the velocity analysis tool was applied

to the data of the complete run to estimate the global average reflection amplitude of that particular run. Further, the identified regions of higher contrast or locations of possible de-bonding were cropped using the edit block tool, and these files were saved separately. These cropped files or ‘blocks’ were further processed using the velocity analysis tool to estimate that particular block’s average reflection amplitude.

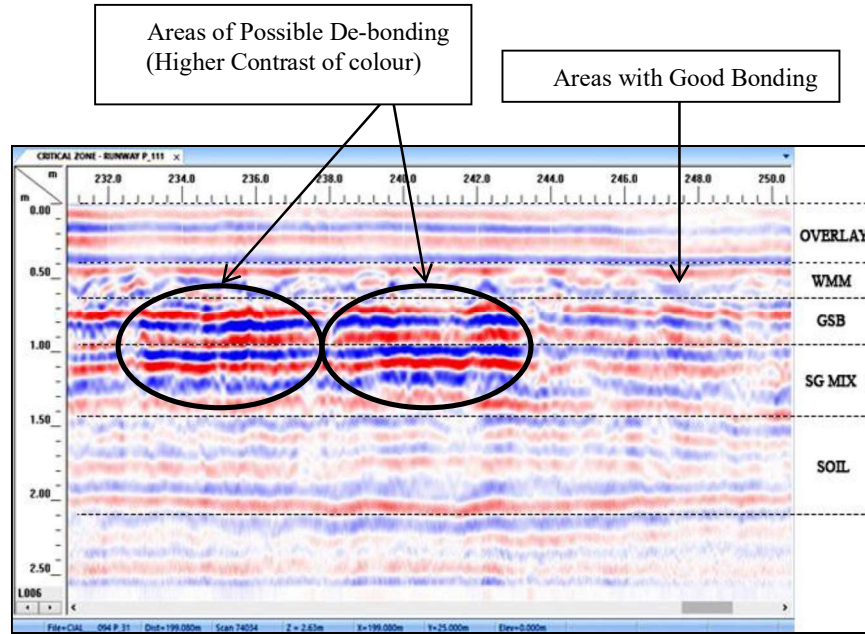


Fig.4. Processed data file showing areas of possible de-bonding and good bonding

Finally, the average reflection amplitudes estimated for the block and the run are used to compute the particular block’s stripping index (SI) by applying the values in equation 1 [12].

$$SI_{block} = \frac{\text{Average reflection amplitude of particular block}}{\text{Global average reflection amplitude of the run}} \quad (1)$$

This same procedure was used to calculate stripping indices for blocks identified in all the offset runs in that particular segment. Where the global average reflection amplitude of the segment is the average of average reflection amplitudes of the individual runs within the segment.

$$SI_{run} = \frac{\text{Average reflection amplitude of particular run}}{\text{Global average reflection amplitude of the segment}} \quad (2)$$

Similarly, the stripping index of each segment was estimated by,

$$SI_{segment} = \frac{\text{Average reflection amplitude of particular segment}}{\text{Global average reflection amplitude of complete runway}} \quad (3)$$

Where the global average reflection amplitude of the complete runway is the average reflection amplitude of the runway’s individual segments. A similar procedure was adopted to estimate stripping indices of blocks, runs, and segments in the taxiway and linkways.

The estimated values of the stripping index are relative as they are dependent on the characteristics that are site-specific. Therefore, the higher the stripping index value implies, the greater the de-bonding than the other identified de-bonding locations. The stripping index values of particular blocks are compared to the overall normalized stripping index to conclude the comparative severity of debonding in each block. In this case study, the severity rating of the de-bonding has been classified, as shown in Table 1.

Table 1. Relationship between Stripping Index and De-bonding Rating

Stripping Index	De-bonding Rating
0 – 0.8	No de-bonding
0.8 – 1.0	Slight de-bonding
1.0 – 1.5	De-bonding

Further, all the blocks noted in a segment were checked for identical chainage, and depth co-ordinates across the segments running parallel to it. Such verification was done to map the flow of the damages along the width of the pavement. If any such identical blocks exist, the corresponding runs and co-ordinates are noted. A sample of the blocks identified in a run along with their assigned stripping indices is shown in figure 5.

3080-3330				
FILE NO: CIAL_100 (CENTER)				
S.No	CH	DEPTH	ANOMOLY	UTILITY
1	3296-3294	0.4-1.3	1.45	
2	3278	0.3		
3	3277	0.3		
4	3238	0.3		
5	3227-3225	0.9-1.3	0.91	
6	3200-3182	0.6-1.1	0.85	
7	3181-3175	1.0-1.4	0.83	
8	3175	0.1		
9	3167-3162	1.0-1.4	0.91	
10	3124-3117	0.9-1.3	0.92	
11	3090	0.5		
12	3088-3080	0.9-1.2	0.95	





INDEX	
	Minor Utility
	Major Utility
	0.8-1 Slight Debonding
	1.1-1.5 Debonding

Fig.5. Sample Tabulation Details of a Run

The identical approach was applied to identify areas of debonding and estimate stripping indices in all the runway, taxiway, and link-ways segments. The various corresponding individual segments were appended to develop a graphical 3D representation of the complete runway, taxiway, or link-ways.

9 Data Interpretation

The utilities identified using the migration tool was tabulated with respect to the corresponding chainage and depth. They were classified as major and minor utilities based on the diameter. The path of the utility can be identified when the processed data files are appended as a 3D file.

The average reflection amplitude value of each run in a segment was used to compute the average reflection amplitude of the particular segment. Similarly, average reflection amplitude values were computed for all the segments, which were further used to calculate the global average reflection amplitude for the corresponding runway, parallel taxiway, or link-way. This global average reflection amplitude was used to compute the stripping indices for the individual segments.

Based on these computed stripping indices, it was observed that the segments 8 and 9 of the 14 segments of the runway were expected to have more debonding with values greater than 1.1. Likewise, segments 8 and 9 were also expected to have more debonding in the parallel taxiway with values greater than 1. Among the various link-ways, C3 and Delta were expected to have more debonding due to flood since the estimated stripping indices are 1.12 and 1.09, respectively. A sample cross-section taken from segment 8, showing a pictorial representation of the de-bonded region along with the depth, is shown in figure 6.

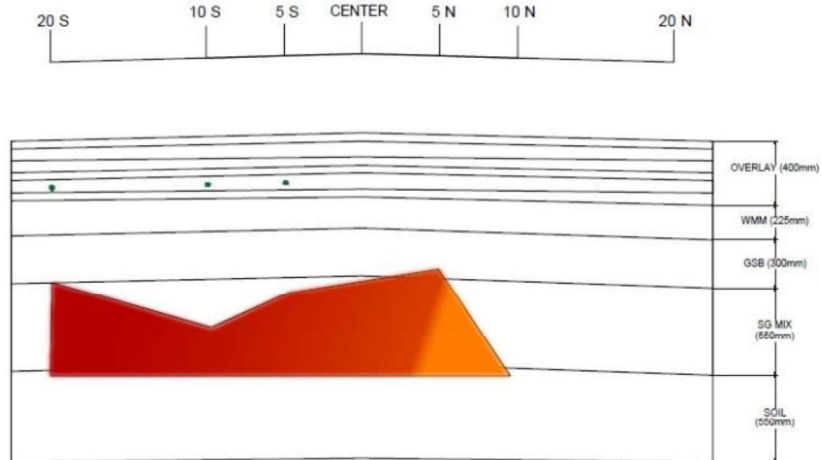


Fig.6. The Cross-Section Showing Location and Degree of De-bonding

The above figure clearly shows the cross-section of the pavement structure with its various layers. Also, it shows the degree of the damages caused by the natural calamity. We can observe the flow of the damage caused by the flooded waters based on the colour coding. The red represents the high de-bonding, and orange represents slight de-bonding. The damage appears extreme at entry from the South of the pavement, and the degree of damage reduces as it moves towards the center. The layers of the pavement structure, which are subjected to damage, can also be observed in figure 6. Therefore, it can be concluded that with a systematic GPR survey, any damages on the pavement or the subgrade can be estimated, and the degree of damages can also be mapped accurately.

The processed individual segment data are appended to develop a complete graphical 3D representation of the corresponding runway, taxiway, or the link-way. Such graphical representations can be used to observe the path of utility and the region of debonding along with the depth. A typically developed 3D-file for a segment of the runway is shown in figure 7.

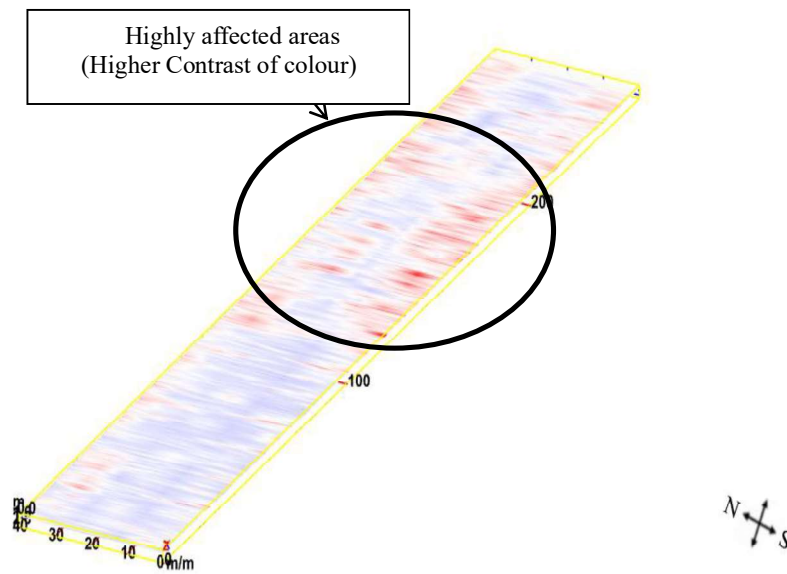


Fig.7. Graphical 3D Representation of a Typical Segment

Figure 7 shows the wholly mapped 3D file of segment 8 of the runway. The GPR survey planned as a grid pattern was ideal for the development of this 3D plot. Such a complete mapping of the site provides us a comprehensive understanding of the damages that have occurred and serves as an ideal reference for further rehabilitation measures to be planned.

In this case, the image's depth is also focused on the depth where most affected locations were observed, which lay between 1 to 1.5 meters from the ground level. Here, we can observe the majorly affected areas lying between 100m and 200m with a higher contrast of colour.

10 Conclusions

The case study presented in this manuscript documents the Ground Penetrating Radar survey application to estimate qualitatively and quantitatively the de-bonding/damages on the pavement and its underlying layers, including the subgrade caused by prolonged interaction of moisture. As a result of this subsurface exploration, the de-bonding locations were graphically mapped, and the degree of de-bonding was numerically tabulated.

1. The Ground Penetrating Radar as a non-destructive test provides a comprehensive understanding of the site's subsurface even under extremely restricted conditions regarding time and accessibility to the site.
2. The subsurface survey employing GPR deduces the areas of water-clogging and material de-bonding beneath the pavement surface along with an estimate of the degree of the damage at each identified location.
3. The estimated numerical values of the 'Stripping Index' provide a clear idea of the region, which is relatively highly affected by de-bonding/damages and requires immediate rehabilitation.
4. The GPR radargram can help in identifying any intermixing of layers beneath the surface of the pavement.

Acknowledgement

The authors would like to acknowledge the Cochin International Airport Limited (CIAL) for providing the opportunity to conduct this work and for extending their support for its execution.

References

1. Gizzi, F. T., and G. Leucci. (2018), "Global research patterns on ground penetrating radar (GPR)," *Surv. Geophys.* 39 (6): 1039–1068. <https://doi.org/10.1007/s10712-018-9475-1>.
2. Davis, J.L., Annan, A.P., (1987) "Ground Penetrating Radar for high-resolution mapping of soil and rock stratigraphy," *Geophysical Prospecting* 37, pp. 531 – 551.
3. Wright, D.L., Olhoeft, G.R., and Watts, R.D. (1984), "Ground Penetrating Radar Studies on Cape Cod," *Proceedings on the NWWA/EPA Conference on Surface and Borehole Geophysical Methods in Ground Water Investigations*, San Antonio, TX, pp. 666-680.
4. Beres, M., and Haeni, F.P., (1991), "Application of Ground-Penetrating Radar Methods in Hydrogeologic Studies," *Ground Water*, Vol 29, No. 3, pp. 375-386.
5. Imse, J.P., and Levine, E.N., (1985), "Conventional and State-of-the-Art Geophysical Techniques for Fracture Detection," *Proceedings Second Annual Eastern Regional Ground Water Conference*, National Water Well Association, Portland, ME pp. 261-276.

Kasinathan Muthukkumaran, Nandhagopal Raj, and Umanath Umaiyan

6. Ulriksen, C.P.F. (1982), "Application of Impulse Radar to Civil Engineering, Ph.D. Thesis, Department of Engineering Geology," Lund University of Technology, Sweden, pp 175.
7. Al-Qadi, I. L., Lahouar, S., Jiang, K., McGhee, K., Mokarem, D., (2005), "Validation of Ground Penetration Radar Accuracy for Estimating Pavement Layer Thicknesses," Paper No. 05-2341, Proceedings, Transportation Research Board 84th Annual Meeting, Washington, DC.
8. Maser, K. R., (1999) "Pavement Characterization Using Ground Penetrating Radar: State of the Art and Current Practice," Non-destructive Testing of Pavements and Back-calculation of Moduli: Third Volume, ASTM STP 1375, American Society for Testing and Materials, West Conshohocken, PA.
9. Wenzlick, J., Scullion, T., and Maser, K.R. (1999) "High Accuracy Pavement Thickness Measurement using Ground Penetrating Radar," Report No. RDT 99-003, Missouri Dept. of Transportation.
10. Wu, B., Ji, Y., and Fang, G. (2010), "Analysis of GPR UWB half-ellipse antennas with different heights of backed cavity above ground," IEEE Antennas Wireless Propagation Lett. 9 (Mar): 130–133. <https://doi.org/10.1109/LAWP.2010.2044475>.
11. Saarenketo, T., Scullion, T. (2000), "Road Evaluation with Ground Penetrating Radar," Journal of Applied Geophysics 43, pp 119 - 138.
12. Ground Penetration Radar Evaluation of Pavement Stripping at Runway 22L, Logan Airport, (2006), Final Report submitted by Infrasense Inc., Arlington, MA to Edward and Kelcey, Boston, MA.
13. Reynolds, M. (1997), "An Introduction to Applied and Environmental Geophysics," John Wiley & Sons, New York.
14. GSSI SIR 3000 manual (2003), Geophysical Survey Systems, Inc., 40 Simon Street Nashua, New Hampshire, USA.
15. Savuth, C. (2006) "Contribution à l'auscultation structurelle des chaussées mixtes: détection des défauts d'interface à l'aide de la deflexion". Ph D Thesis. INSA de Rennes. France.
16. Hammons, M., Maser, K., and von Quintus, H. (2005). "Detection of Stripping in Hot Mix Asphalt" Final Report prepared for the Georgia DOT Office of Materials and Research.